Studies of the CEA Design Proposals for EU-DEMO Magnets

A. Torre, C. NGuyen Thanh Dao, Q. Le Coz, P. Hertout, L. Zani, F. Villecroze, B. Boudes, A. Nijhuis, R. Lubkemann, and V. Corato

***Abstract*—The paper gives an overview of the latest magnet design activities at CEA for the EU-DEMO Magnet Systems. It explains the latest changes in design constraints, inputs and definitions, the updates that have been implemented in the design tools, and shows the latest CEA proposed design for the TF magnet. We will discuss the recent updates in the TF and PF design tools which were used in 2022 and 2023. In particular, the tools have evolved to include additional constraints or operating points like possible sub-cooling of the coils or synchronous discharge of the axisymmetric PF/CS system. The electromagnetic coupling of the TF coils with coil case and radial plates is also discussed during a fast safety discharge, along with energy extraction and deposition sharing. Furthermore, a new 2D TF mechanical model is presented that permits to make a fast iteration with design tools and optimize the radial build. Finally, the paper also includes an update on the CEA TF conductor qualification sample, describing in particular the latest results obtained in the Twente Press.**

***Index Terms*—DEMO, design, superconducting magnets.**

I. Introduction

SINCE 2020, CEA designs and proposes a conductors and winding packs designs for the EU-DEMO WPMAG activities (see [1], [2], [3] and [4]). The task involves a fast evaluation of new design points with constraints that evolve along the years. This paper will present the overall design results obtained in 2022-2023 for the TF-WP4 option, with radial plates (RP), and PF coils, describing all changes introduced in the design tool to decrease the discharge voltage and limit the superconducting strand amount.

II. TF-WP4 Magnet Design – Inputs & Changes

A. Introduction

Since no major change in the overall Eurofusion DEMO baseline was introduced in 2022, we focused our design efforts on the update of design hypotheses in the CEA design tool MADMACS. These changes were also introduced to be in accordance with the design hypotheses listed in the WPMAG Common Memo [5], like the reference strand scaling law (WST with −0.5% effective strain). Other important changes are described and their impact is discussed in the following paragraphs.

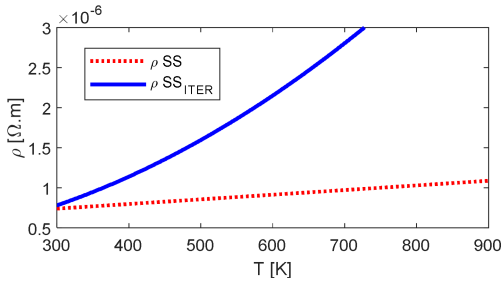

Fig. 1. Comparison of material resistivity for dump resistors. Standard SS is in dashed red, ITER material is in plain blue.

B. Discharge Circuit and Dump Resistor

Each coil is now foreseen to be discharged on a dedicated dump resistor with a mid-point to ground, which limits the discharge voltage to about half of what it was in previous designs.

Furthermore, the dump resistor material properties have been updated. Indeed, until 2021, the resistors were designed in standard stainless steel. We introduced, as a modification in the MADMACS tool, the material properties of the steel used for the ITER dump resistors (partially described in [6]). This material's resistivity ρ has a very large thermal sensitivity so that the dump resistance increases during the discharge. The comparison of ρ versus temperature is made on Fig. 1 between standard stainless steel (SS) and the ITER material.

Using this type material has a beneficial effect: it accelerates the discharge without increasing the initial voltage, decreasing de-facto the needed cooper content of the conductor.

C. Radial-Plates Potential and Insulation

When the radial-plates option for the TF winding pack was recommended to be studied in 2020, the requirements for insulation thicknesses was not completely clear because it had been defined in the Common Memo [5] for winding packs without RP as: ground insulation (8 mm), pancake to pancake insulation (4 mm), turn-to-turn insulation (2 mm). But in the case where the radial plates define a single potential in front of all turns of a pancake, some were recommending that we use the full 8 mm ground insulation for each conductors. In reality, as it is done in

Manuscript received 21 September 2023; revised 20 December 2023; accepted 29 January 2024. Date of publication 12 February 2024; date of current version 26 February 2024. This work was supported by EUROfusion Consortium, funded by the European Union through the Euratom Research and Training Programme under Grant 101052200—EUROfusion. *(Corresponding author: A. Torre.)*

A. Torre, C. NGuyen Thanh Dao, Q. Le Coz, P. Hertout, L. Zani, F. Villecroze, and B. Boudes are with CEA Cadarache, IRFM, 13108 St-Paul Lez Durance Cedex, France (e-mail: alexandre.torre@cea.fr).

A. Nijhuis and R. Lubkemann are with the Faculty of Science and Technology, University of Twente, 7500AE Enschede, The Netherlands.

V. Corato is with ENEA, I-00044 Frascati, Italy.

Color versions of one or more figures in this article are available at https://doi.org/10.1109/TASC.2024.3362750.

Digital Object Identifier 10.1109/TASC.2024.3362750

TABLE I
CONDUCTOR DESIGN OUTPUTS

Name	Value	Description
$\mathbf{I_{op}}$	116.55 [kA]	Operating current
$\mathbf{N_{Sc}}$	721 [-]	Number of Sc Strands
$\mathbf{N_{Cu}}$	1108 [-]	Number of Cu Strands
$\mathbf{D_{cab}}$	54.92 [mm]	Cable Diameter
$\mathbf{d_{jack}}$	2 [mm]	Jacket Thickness

ITER, the radial plate is electrically connected to the middle of a double pancake, so that the maximum conductor to RP voltage can be kept to: $V_{cond-RP} = V_{\max}/(2N_{2pck})$

Where $V_{\max}$ is the design maximum voltage to ground, here 5 kV, and $N_{2\mathrm{pck}}$ is the number of double pancakes in the WP. To be consistent with the ITER insulation scheme, we thus proposed to rely on 2 mm glass-kapton half-overlapped insulation (1.25 mm in ITER). This is highly conservative considering that the ITER design voltage to ground for the TF coils is 7 kV [7].

D. Conductor Copper Resistivity

During the TF discharge, the amount of copper content in the conductor, either as segregated strands or inside the superconducting strands, should be computed so that the hotspot criterion ($T_{hotspot}$<250 K, see [5]) is maintained. But as described in the Common Memo [5], it is possible to consider segregated copper strands with a RRR up to 400 and the copper inside the superconducting strands with a RRR of 100. We refined our design tool by defining an equivalent copper resistivity $\rho_{Cu\text{-}eq}$ (in a similar way than proposed in [8]) that takes into account those two types of copper in parallel:

$$\rho_{Cu-eq} = \frac{\rho_{Cu}^{100} * \rho_{Cu}^{400} * (S_{100} + S_{400})}{(S_{100}\,\rho_{Cu}^{400} + S_{400}\,\rho_{Cu}^{100})}$$

With ρ_{Cu}^{RRR} The resistivity of copper for a given RRR, and S_{RRR} the associated cross-section in the cable. This permitted areduction of the copper content of the cable.

III. TF-WP4 MAGNET DESIGN – RESULTS & ANALYSIS

A. Updated TF-WP4 Design

The main design inputs were an operating temperature (T_{op}) of 4.7 K, a maximum field ($B_{\max}$) of 12.27 T, a temperature margin (ΔT_m) of 1.5 K and a total available housing space for the winding pack of 1.29 m (toroidally) by 0.63 m (radially). Table I presents the updated design with regards to the conductor design characteristics.

The resulting WP design is an 8 turns by 8 double pancakes coil with an inducance of 1.38 H, and a total mass of superconducting strands of 604 tons. It is illustrated in Fig. 2.

One can see on this figure that a grading of the stainless thicknesses was introduced to optimize the SS cross-section. The design has a hotspot temperature of 250 K, and a maximum voltage during discharge of 3 kV to ground (for $R_{dump} = 39.4$ mΩ). The preliminary mechanical analysis made in MADMACS (0D in-plane forces, see [9]) leads to 660 MPa in the casing nose and 739 MPa in the conductor jacket. This last value, although above criteria, is known to be conservative (see details in [10]) and is updated in the 2D mechanical analysis.

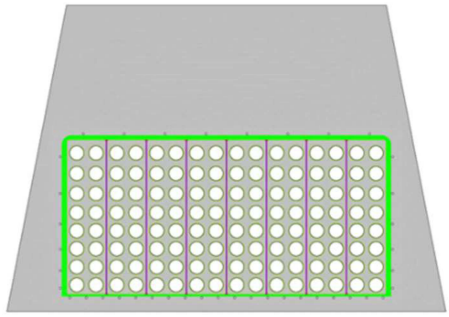

Fig. 2. 2022 baseline design of TF-WP4 with radial plates.

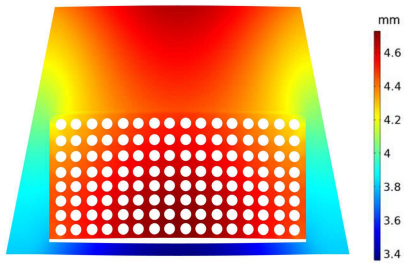

Fig. 3. Mechanical analysis: displacements due to J × B volumic forces.

B. 2D Mechanical Analysis

In this paragraph we report the 2D detailed mechanical analysis of the TF-WP4 inner leg. The study was performed using a multi-physics ©COMSOL model with Lorentz Loads defined by the magnetic field map computed. The results are shown in Fig. 3 in terms of displacement (right).

The stress in the casing has punctual high values, but once averaged over standard critical linearization paths, as discussed in [12] and [13], the maximum membrane (P_m) plus bending (P_b) stress in the casing is found to be around ${\sigma^{max\text{-}cas}}_{m+b} =$ 520 MPa, below the Tresca 660 MPa criteria.

Inside the radial plates and conductor jackets, we observe stress concentration on the external part of the WP, due to the cumulative load of the conductors. In this case, after linearization along the paths, one gets ${\sigma^{max\text{-}RP}}_{m+b} = 566$ MPa and ${\sigma^{max\text{-}jack}}_{m+b} = 609$ MPa, also below criteria. This analysis points out that there is still some margin in the mechanical design, which will be necessary to cope with the additional out-of-plane loads to be studied in the future.

Compressive and shear stress analysis in the insulating parts of the WP have also been made showing an overall good insulation mechanical behavior (see Fig. 4). It should be said that some insulating areas are subject to relatively high debonding fracture according to LHD criteria [10]. This is mainly due to the radial force being transformed by the vault of the coils into toroidal compression (and bending of the case cover).

C. Magnetic Coupling During Discharge

The energy ${E_{mag}}^{TF}$ stored in the TF system in its 2022–2023 version is about 149 GJ. During the system fast safety discharge (FSD) in 35 s, the main part of the energy is extracted in the dump resistors. Nevertheless, a small part is magnetically coupled to the radial plates (RP), to the casing (CAS) and to the vacuum vessel (VV). Solving the standard differential equation

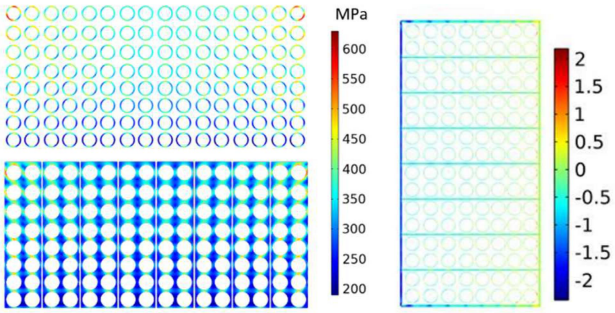

Fig. 4. Mechanical analysis: Stress in the radial plates and conductor jackets (left) and LHD criteria in insulation (right).

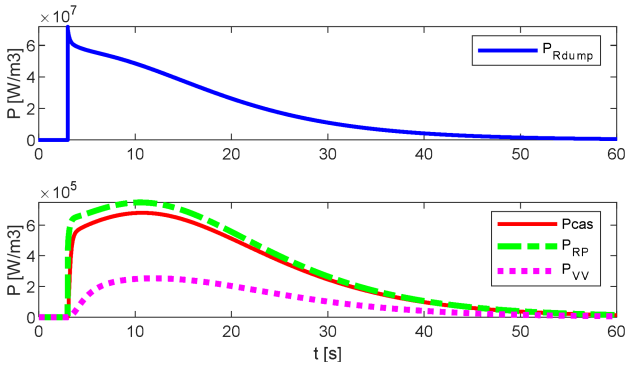

Fig. 5. Power versus time for the magnetically coupled elements during FSD.

LM.I'+RI = 0 with LM the self and mutual inductances matrix and R the resistances of the various components we can find the currents waveforms, thus the power, and finally total sharing of the energy between the various elements by integration. Fig. 5 shows the power versus time during the current dump. In the end the energy sharing between elements is: 81% (121 GJ) in the dump resistors, 9% (13 GJ) in the coil cases, 6% (9.3 GJ) in the VV and 4% (6.2 GJ) in the radial plates.

Although small in percentage compared to the total energy, in absolute values the coupled energy is far from negligible and will trigger important temperature increases. A preliminary adiabatic calculation was made which indicates that the case and RP could heat up to about 50 K during FSD, probably triggering a quench of the magnet during discharge.

D. Maximum Voltage During Discharge

When we first computed in MADMACS, which does not include the magnetic coupling, the maximum voltage during FSD, we were surprised to see that the maximum voltage was not appearing at the start of the discharge. Indeed, since the new material for the dump resistor has such a large sensitivity with temperature, the increase in resistance goes faster than the current dump. Nevertheless, the magnetic coupling study made afterwards showed that enough current is immediately coupled from the coil to the structures so that the initial voltage is also immediately lowered (see Fig. 6).

The two curves, with and without magnetic coupling, are reported in Fig. 6, showing the immediate effect at the start of the FSD, plus a dampening effect on the voltage rise.

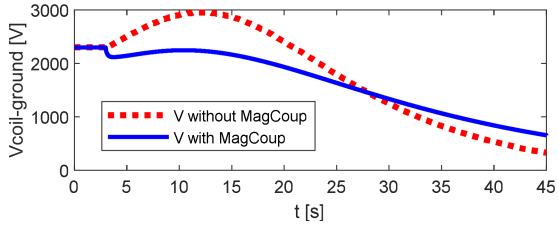

Fig. 6. Effect of magnetic coupling on the maximum voltage during FSD (without coupling in red dashed, with coupling in plain blue).

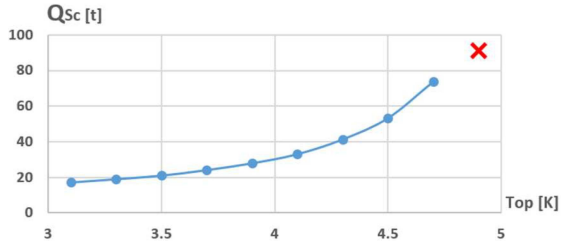

Fig. 7. Fixed geometry parametric study on strand quantity versus operating temperature.

IV. PF Coils Studies

A. Previous Design and Sub Cooling

The initial design study for CEA PF coils had led us to consider high aspect ratio coils (vertically) if we wanted to keep NbTi as base material for all coils and a single 1 km conductor length for each double pancake. The design is reported in [4] and had a number of advantages in terms of maximum field on the coil and thus in terms of superconducting strands amount. For PF1 for example, the strand quantity (in tons) was found to scale with aspect ratio (AR) as $Q_{sc} = -5.36AR+41.7$ for aspect ratio between 3 and 6 due to the local decrease of the maximum magnetic field.

The study presented here, with the same tool as in [4], is a simple sub-cooling parametric sweep, in fixed geometry, showing the impact of the lower operating temperature on the overall PF system NbTi strands quantity. The plot in Fig. 7 shows that the region with high net gain of sub-cooling is thus between 4 K and 4.7 K, although below 4 K the gain is still interesting.

B. Lower AR and New Baseline

Nevertheless, having these large aspect ratios also had drawbacks in terms of manufacturability and clash with the TF coils cases. Furthermore, there was the potential drawback of having the coils centerline further away from the plasma, thus lowering the efficiency of the coils.

To lower the AR to about 2 (similar to ITER) while keeping NbTi, we need to introduce 2-in-hand or 4-in-hand (or internal joints) windings. Furthermore, based on previous sub-cooling studies [14], we allowed T_{op} to be lowered down to 3 K, in a region where there is a potential gain in overall magnet and cryogenic investment plus operating cost. Finally, we needed to take into account the magnetic coupling of the PF system during FSD, which was made by defining a unique dump time constant ${\tau_{dis}}^{PF}$ of 24 s (synchronous discharge). Introducing these modifications, we defined a new PF baseline, summarized in Table II.

TABLE II
NEW PF BASELINE (3 K, 2-IN-HAND)

Name	PF1	PF2	PF3	PF4	PF5	PF6
B_{max} [T]	6.73	3.33	4.81	5.18	4.28	7.33
N_{trn} [-]	13	8	8	8	10	16
N_{pck} [-]	26	16	22	32	20	32
N_{Sc} [-]	188	65	94	102	84	242
N_{Cu} [-]	1113	1082	1137	1109	1172	1028
I_{cond} [kA]	48.9	46	48.1	47	49.5	46.9
L_{cond} [mm]	56.5	53.1	45.6	45.1	56.1	54.5
L [H]	1.91	1.14	2.89	5.72	2.58	5.86
Q_{sup} [tons]	3.24	1.1	2.8	4.43	2.22	8.18

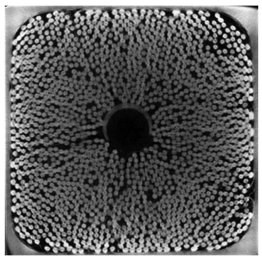

Fig. 8. Tomographic cross-section of TF square-in-square CEA TF conductor (courtesy INFLPR).

TABLE III
TWENTE PRESS TEST CONDITIONS

Top	B_{app}	F_{nom}	F_{app}	#cycles	f_{max}
[K]	[T]	[kN/m]	[kN/m]	[-]	[Hz]
4.2	0.35 +/-0.15	891	445	34000	0.16

V. TF-WP4 CONDUCTOR UPDATE

A. Introduction

A square-in-square conductor, representative of a TF wind and react (W&R) conductor was manufactured in 2021, is described in [1] and illustrated by an X-ray tomography in Fig. 8 (courtesy National Institute for Laser, Plasma and Radiation Physics: INFLPR, Romania).

The final goal is to qualify the conductor in SULTAN facility and test its performances, but due to some manufacturing issues it is not yet tested. In the meantime, a short length of it was tested in the Twente Press [15] for ac losses properties. The test conditions are summarized in Table III.

A full mechanical and electrical characterization of the conductor was made. A remarkable point is that the initial (virgin) loading to 445 kN/m triggered a very small cable displacement of 162 µm, indicating high intrinsic cable transverse stiffness. Two other specific measurements are detailed in the following paragraphs.

B. Contact Resistances

The contact resistances (R_C) between strands of various cabling stages are measured, with and without nominal applied load, and along the 34000 mechanical cycles performed. The result is a small increase of R_C and a nice stabilization with cycling. We fitted with good agreement the evolution of R_C with the cycle number N_{cyc} using the following fit:

$$R_C\left(N_{cyc}\right) = R_{C0} + a.\log\left(N_{cyc}\right)$$

The results for the various cabling stages, with and without applied load F_{app}, are reported in Table IV. The overall stabilisation of R_C with cycling is also a good indicator of the cable robustness versus transverse load.

TABLE IV
R_C EVOLUTION WITH CYCLING PARAMETERS

	Intra-triplet		Intra-petal		Inter-petal	
	0kN/m	F_{app}	0kN/m	F_{app}	0kN/m	F_{app}
R_{C0} [nΩ]	3.58	3.45	5.04	4.79	36.46	27.34
α [nΩ/log(N_{cyc})]	0.066	0.096	0.1	0.18	2.96	1.90

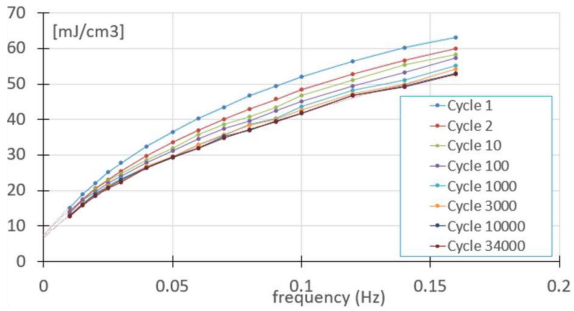

Fig. 9. AC losses versus frequency at various cycling stages in the fully loaded state.

C. AC Losses

The ac losses are measured in Twente Press with and without applied load. The curve versus frequency in the fully loaded state is shown in Fig. 9.

This curve shows that the decrease with cycling of the losses and subsequent time constant is small. This result is very promising in terms of dc performance, and we expect a very robust T_{CS} and I_C behavior versus cycling in SULTAN. Nevertheless, the time constant computed is around 2500 ms, significantly higherthan our past ac losses hypotheses (600 ms in [16]). This result is still under investigation and should be confirmed in the future by comparison to Josefa [17] or SULTAN [18] results.

VI. CONCLUSION

In this paper we presented the design studies led at CEA in 2022–2023, which permitted to propose updated baseline designs for the TF and PF magnets. The TF study permitted to emphasize the importance of the dump resistor material and the magnetic coupling during FSD. The PF study focused on potential sub-cooling possibilities and gains while keeping NbTi as base material. Finally we described the latest results of the TF square in square prototype conductor in the Twente Press. The conductor has a good ac performance which is promising in terms of robustness against transverse load, while maintaining an acceptable time constant for a conductor of this size.

Disclaimer: Views and opinions expressed are however those of the author(s) only and do not necessarily reflect those of the European Union or the European Commission. Neither the European Union nor the European Commission can be held responsible for them.

REFERENCES

[1] V. Corato et al., "The DEMO magnet system – Status and future challenges," *Fusion Eng. Des.*, vol. 174, 2022.

[2] L. Zani et al., "Updates on CEA design and experimental activities on EU DEMO TF system," *IEEE Trans. Appl. Supercond.*, vol. 32, no. 6, Sep. 2022, Art. no. 4203405.

[3] L. Zani et al., "Updates on magnet design for EU-DEMO reactor:Optimization studies on TF and CS systems," *IEEE Trans. Appl. Supercond.*, vol. 31, no. 5, Aug. 2021, Art. no. 4202606.

[4] L. Zani et al., "CEA broad studies on EU DEMO CS and PF magnet systems," *IEEE Trans. Appl. Supercond.*, vol. 30, no. 4, Jun. 2020, Art. no. 4203306.

[5] V. Corato et al., "Common operating values for DEMO magnets design for 2016," 2016. [Online]. Available: https://scipub.euro-fusion.org/wp-content/uploads/eurofusion/WPMAGREP16_16565_submitted.pdf

[6] I. Song et al., "The fast discharge system of ITER superconducting magnets," in *Proc. IEEE Int. Conf. Elect. Machines Syst.*, 2011. pp. 1–6.

[7] S. Fink et al., "High voltage tests of the ITER toroidal field model coil insulation system," *IEEE Trans. Appl. Supercond.*, vol. 12, no. 1, pp. 554–557, Mar. 2002.

[8] M. N. Wilson, *Superconducting Magnets*, Clarendon: Oxford Science Publications, 1983.

[9] A. Torre et al., "Tools used at CEA for designing the DEMO toroidal field coils winding pack," *IEEE Trans. Appl. Supercond.*, vol. 26, no. 4, Jun. 2016, Art. no. 4902005.

[10] K. Kitamura et al., "Cryogenic shear fracture tests of interlaminar organic insultation for forced flow superconducting coil," *IEEE Trans. Magn.*, vol. 30, no. 4, pp. 1879–1882, Jul. 1994.

[11] A. Panin et al., "Analysis approaches to resolve structural issues of the European DEMO toroidal field coil system at an early design stage," 2015. [Online]. Available: https://scipub.euro-fusion.org/wp-content/uploads/2015/11/EFCP150905.pdf

[12] F. Nunio et al., "Mechanical analysis of the European DEMO central solenoid pre-load structure and coils," *Fusion Eng. Des.*, vol. 146, pp. 168–161, 2019.

[13] V. Corato et al., "Progress in the design of the superconducting magnets for the EU DEMO," *Fusion Eng. Des.*, vol. 136, pp. 1597–1604, 2018.

[14] L. Zani, "Development of a multi-physic platform OLYMPE for magnet fusion design: Progresses update and applications," *Cryogenics*, vol. 125, 2022, Art. no. 103479.

[15] K. Yagotintsev, "AC loss, interstrand resistance and mechanical properties of prototype EU DEMO TF conductors up to 30 000 load cycles," *Supercond. Sci. Technol.*, vol. 31, no. 2, Dec. 2017, Art. no. 025010.

[16] Q. Le Coz et al., "TACTICS: Overview of a multi-physic analysis tool for fusion magnet design and application to DEMO TF coil," *Cryogenics*, vol. 127, Oct. 2022, Art. no. 103553.

[17] M. Chiletti, J.-L. Duchateau, F. Topin, B. Turck, and L. Zani, " Void fraction influence on CICCs coupling losses: Analysis of experimental results with MPAS model," *IEEE Trans. Appl. Supercond.*, vol. 30, no. 4, Jun. 2020, Art. no. 4701405.

[18] P. Bruzzone et al., "Upgrade of operating range for SULTAN test facility," *IEEE Trans. Appl. Supercond.*, vol. 12, no. 1, pp. 520–523, Mar. 2002.